An evaluation of CALIOP/CALIPSO's aerosol-above-cloud detection and retrieval capability over North America

M. Kacenelenbogen,[1] J. Redemann,[2] M. A. Vaughan,[3] A. H. Omar,[3] P. B. Russell,[2] S. Burton,[3] R. R. Rogers,[3] R. A. Ferrare,[3] and C. A. Hostetler[3]

Received 8 May 2013; revised 4 November 2013; accepted 10 December 2013; published 15 January 2014.

[1] Assessing the accuracy of the aerosol-above-cloud (AAC) properties derived by CALIOP (the Cloud-Aerosol Lidar with Orthogonal Polarization) is challenged by the shortage of accurate global validation measurements. We have used measurements of aerosol vertical profiles from the NASA Langley airborne High Spectral Resolution Lidar (HSRL-1) in 86 CALIOP-coincident flights to evaluate CALIOP AAC detection, classification, and retrieval. Our study shows that CALIOP detects ~23% of the HSRL-detected AAC. According to our CALIOP-HSRL data set, the majority of AAC aerosol optical depth (AOD) values are < 0.1 at 532 nm over North America. Our analyses show that the standard CALIOP retrieval algorithm substantially underestimates the occurrence frequency of AAC when optical depths are less than ~0.02. Those aerosols with low AOD values can still have a consequent radiative forcing effect depending on the underlying cloud cover and overlying aerosol absorption properties. We find essentially no correlation between CALIOP and HSRL AAC AOD ($R2 = 0.27$ and $N = 151$). We show that the CALIOP underestimation of AAC is mostly due to tenuous aerosol layers with backscatter less than the CALIOP detection threshold. The application of an alternate CALIOP AAC retrieval method (depolarization ratio) to our data set yields very few coincident cases. We stress the need for more extensive suborbital CALIOP validation campaigns to acquire a process-level understanding of AAC implications and further evaluate CALIOP's AAC detection and retrieval capability, especially over the ocean and in different parts of the world where AAC are more frequently observed and show higher values of AOD.

Citation: Kacenelenbogen, M., J. Redemann, M. A. Vaughan, A. H. Omar, P. B. Russell, S. Burton, R. R. Rogers, R. A. Ferrare, and C. A. Hostetler (2014), An evaluation of CALIOP/CALIPSO's aerosol-above-cloud detection and retrieval capability over North America, *J. Geophys. Res. Atmos.*, *119*, 230–244, doi:10.1002/2013JD020178.

1. Introduction

[2] The presence of aerosol above clouds (AAC) can interfere with the ability of passive instruments to accurately determine cloud optical properties [*Haywood et al.*, 2004; *Wilcox et al.*, 2009; *Coddington et al.*, 2010]. *Coddington et al.* [2010] found that an overlying absorbing aerosol layer biases Solar Spectral Flux Radiometer (SSFR) cloud retrievals toward smaller effective radii and optical depth while nonabsorbing aerosols had no impact. In particular, a light-absorbing aerosol layer above bright clouds can significantly darken a scene. AAC can increase the amount of incoming solar radiation absorbed by the atmosphere and decrease the amount of solar radiation reflected back to space. The diurnal average radiative flux-change approximations of *Haywood and Shine* [1995], *Chylek and Wong* [1995], and *Russell et al.* [1997, 2002] show that the aerosol-induced change in upwelling flux at the top of atmosphere is a function of the aerosol type, the cloud fraction, and the underlying surface albedo, among other parameters. Recent studies [*Chand et al.*, 2009; *Remer*, 2009; *Koch and Del Genio*, 2010; *Wilcox*, 2010] define a critical underlying cloud fraction at which AAC switches from exerting a net cooling to a net warming effect of the Earth-atmosphere system: The greater the cloud cover below the aerosols, the more likely the aerosols are to exert a positive forcing (i.e., a warming effect). Let us note that the critical underlying cloud fraction itself depends on the aerosol properties (especially absorption) and the cloud albedo. Thus, an accurate detection and quantification of AAC is of utmost importance for aerosol-climate studies under all-sky conditions, both on regional and global scales [*Sakaeda et al.*, 2011].

[3] Several passive spaceborne sensors are, in principle, able to separate the aerosol and cloud information in the radiation measured at the top of the atmosphere. *Yu and Zhang* [2013]

[1]Bay Area Environmental Research Institute, Sonoma, California, USA.
[2]NASA Ames Research Center, Moffett Field, California, USA.
[3]NASA Langley Research Center, Hampton, Virginia, USA.

Corresponding author: M. Kacenelenbogen, Bay Area Environmental Research Institute, Sonoma, CA 95476, USA. (meloe.s.kacenelenbogen@nasa.gov)

2169-897X/14/10.1002/2013JD020178

Table 1. Description of the Colocated HSRL-CALIOP Data Set by Field Campaign, Date, Location, Number of Flights, and Number of Hours on the CALIOP Track[a]

Mission	Date	Location	Number of CALIOP Flights	Number of Hours on CALIOP Track
CC-VEX	Jun–Aug 2006	Eastern U.S.	11	16.2
TexAQS/GOMACCS	Aug–Sept 2006	Texas	10	13.8
CHAPS	Jun 2007	Oklahoma City area	8	10.9
CATZ	Jul–Aug 2007	Eastern U.S.	4	7.6
CARIBBEAN	Jan–Feb 2008	Caribbean	7	13.2
ARCTAS (spring)	Apr–2008	Alaska	12	17.5
ARCTAS (summer)	Jun–Jul 2008	Canada	11	10.3
Nighttime calibration	Jan–Apr 2009	Eastern U.S.	11	15.9
RACORO	Jun–2009	Oklahoma	3	4
Other	2007–2009	North America	9	6.3
Total			86 flights	115.7 h

[a]Modified from *Rogers et al*. [2011]. The flights grouped in the "other" section of Table 1 were conducted during transit flights to or from NASA LaRC.

describe these AAC retrieval techniques in more detail. For example, aerosols can be measured above clouds using the POLarization and Directionality of Earth Reflectances (POLDER) instrument. The presence of aerosols can significantly affect polarized light reflected by underlying clouds in specific scattering-angle ranges [*Waquet et al*., 2009; *Knobelspiesse et al*., 2011; *Waquet et al*., 2012]. Furthermore, specific aerosols with an absorption optical depth that decreases strongly with wavelength (e.g., in smoke and dust plumes) can be measured above clouds using the Ozone Monitoring Instrument (OMI) [*Torres et al*., 2012]. As an extension to the visible spectral region of the near-UV retrieval technique of *Torres et al*. [2012], *Jethva et al*. [2013] developed a technique to detect and derive the aerosol-above-cloud optical depth and underlying cloud optical depth from the MODerate resolution Imaging Spectroradiometer (MODIS) spectral reflectance measurements. *Yu et al*. [2012] have examined the feasibility of combining OMI aerosol index and MODIS cloud optical depth to derive AAC optical depth. *De Graff et al*. [2012] use the SCanning Imaging Absorption spectroMeter for Atmospheric CHartographY (SCIAMACHY) to directly derive aerosol-above-cloud direct radiative effects without calculating the AAC Aerosol Optical Depth (AOD). However, all these retrievals are limited research products for which there is a lack of global experimental validation. In addition, these sensors require information about cloud and aerosol vertical distribution to provide an accurate measure of aerosol loading (such as AOD). This is typically provided by the Cloud Aerosol LIdar with Orthogonal Polarization, CALIOP, or from differential absorption measurements in the oxygen A-band [*Waquet et al*., 2012]. CALIOP is the only active spaceborne sensor providing aerosol backscatter and inferring extinction profiles in both cloud-free and cloudy conditions [*Winker et al*., 2009]. The advantages of lidar-derived properties near and above clouds are high vertical and temporal resolutions paired with a narrow source of illuminating radiation, which limits cloud adjacency effects (3-D cloud radiative effects) and cloud contamination of data products [*Zhang et al*., 2005; *Wen et al*., 2007; *Várnai and Marshak*, 2009]. Validating products such as the CALIOP AAC occurrence, AAC altitude, geometrical thickness, and optical depth is challenged by the lack of suitable validation data sets. To the best of our knowledge, the existing peer-reviewed evaluations of CALIOP aerosol detection and optical properties retrievals have been largely restricted to cloud-free conditions [*Kim et al*., 2008; *Pappalardo et al*., 2010; *Omar et al*., 2009; *Kacenelenbogen et al*., 2011; *Rogers et al*., 2011; *Burton et al*., 2013; *Winker et al*., 2013; R. R. Rogers et al., manuscript in preparation, 2014]. Nevertheless, CALIOP profiles of attenuated backscatter are used to quantify frequency of occurrence, vertical separation, and zonal and global seasonal means of AAC AOD [*Yu et al*., 2013; *Devasthale and Thomas*, 2011].

[4] To assess the ability of CALIOP to detect AAC, we use measurements acquired by the NASA Langley Research Center (LaRC) airborne High Spectral Resolution Lidar (HSRL) [*Hair et al*., 2008]. The data used in this study were collected on over 800 flight hours from 10 field missions between 2006 and 2009, many of which have included CALIOP validation flights. We use the same 86 HSRL flights over North and Central America (Table 1) that were used in the extensive quantitative assessment of the CALIOP 532 nm total attenuated backscatter by *Rogers et al*. [2011]. The latter article briefly describes each of the missions listed in Table 1.

[5] We first describe both the CALIOP and HSRL instruments, their measurements, and different aerosol retrieval techniques. We then discuss how the coincident HSRL-CALIOP AAC data set of our study compares to global CALIOP AAC observations; we present the results of the HSRL and CALIOP version 3 standard AAC comparisons and list the potential sources of error in the CALIOP retrievals. We conclude our study by applying an alternate CALIOP retrieval method to the AAC cases in the HSRL-CALIOP colocated data set of Table 1.

2. Data and Method

2.1. Description of CALIOP Standard and HSRL Products

[6] CALIOP, flying on board the CALIPSO (Cloud-Aerosol Lidar and Infrared Pathfinder Satellite Observations) platform as part of the A-Train satellite constellation since April 2006, is a three-channel elastic backscatter lidar. CALIOP measures high-resolution (1/3 km in the horizontal and 30 m in the vertical in low and middle troposphere) profiles of the attenuated backscatter from aerosols and clouds at visible (532 nm) and near-infrared (1064 nm) wavelengths along with polarized backscatter in the visible channel [*Hunt et al*., 2009]. These data are distributed as part of the level 1 CALIOP products. The level 2 products are derived from the level 1 products using a succession of complex algorithms [e.g., *Winker et al*., 2009]. The level 2 retrieval scheme is composed of a feature detection scheme [*Vaughan et al*.,

Table 2. Particulate Extinction-to-Backscatter Lidar Ratio Values in the CALIOP Version 3 Level 2 Data Products and Natural Variabilities Estimated for CALIOP's Subtypes[a]

Aerosol Type	Initial Lidar Ratio (532 nm)
Marine	20 sr ±30% (~6 sr)
Desert dust	40 sr ±50% (~20 sr)
Polluted continental	70 sr ±35% (~25 sr)
Clean continental	35 sr ±45% (~16 sr)
Polluted dust	55 sr ±40% (~22 sr)
Biomass burning	70 sr ±40% (~28 sr)

[a]*Omar et al*. [2005]; *Cattrall et al*. [2005].

2009], a module that classifies features according to layer type (i.e., cloud versus aerosol) [*Liu et al*., 2010] and subtype (e.g., aerosol species) [*Omar et al*., 2009], and, finally, an extinction retrieval algorithm [*Young and Vaughan*, 2009] that estimates aerosol backscatter and extinction coefficient profiles and the total column Aerosol Optical Depth (AOD) based on modeled values of the extinction-to-backscatter ratio (also called S_a) inferred for each detected aerosol layer. Table 2 shows the lidar ratio values and natural variabilities estimated for CALIOP's subtypes in the CALIOP version 3 level 2 data products (see http://www-calipso.larc.nasa.gov/resources/calipso_users_guide/data_summaries/layer/index.php#initial_532_lidar_ratio). The goal of the aerosol typing algorithm is to classify the aerosol so as to constrain the uncertainty in lidar ratio to no more than 30% [*Winker et al*., 2009]. The CALIOP AOD fractional error is similar to the S_a fractional error for small AOD values [*Winker et al*., 2009]. However, as the AOD increases, the AOD fractional error will quickly become much larger than the S_a fractional error. The original measurement requirements defined for the uncertainty on the CALIOP AOD is of 40% [*Winker et al*., 2009].

[7] The High Spectral Resolution Lidar (HSRL) technique implemented in the airborne lidar flown by researchers at NASA's Langley Research Center (LaRC) directly retrieves the vertical profiles of aerosol extinction coefficients and extinction-to-backscatter ratios, without requiring ancillary aerosol measurements or assumptions about aerosol type [*Hair et al*., 2008]. The HSRL technique is employed for the 532 nm wavelength utilizing the iodine vapor filter technique [*Hair et al*., 2001, 2008; *Piironen and Eloranta*, 1994]. The 532 nm backscatter return is split between three optical channels: (1) one measuring the backscatter (predominantly aerosol) polarized orthogonally to the transmitted polarization, (2) one measuring 10% of the molecular and aerosol backscatter polarized parallel to the transmitted polarization, and (3) one passing through an iodine vapor cell which absorbs the central portion of the backscatter spectrum, including all of the Mie (aerosol) backscatter, and transmits only the Doppler/pressure-broadened molecular backscatter. This third channel (the "molecular channel") is used to retrieve the extinction profile, and all three channels are used to retrieve profiles of aerosol backscatter, extinction coefficient, and aerosol depolarization ratio. The HSRL extinction profile is retrieved from the measured attenuated molecular backscatter by taking the derivative of the profile with respect to range and subtracting a model-derived molecular extinction profile. *Hair et al*. [2008]

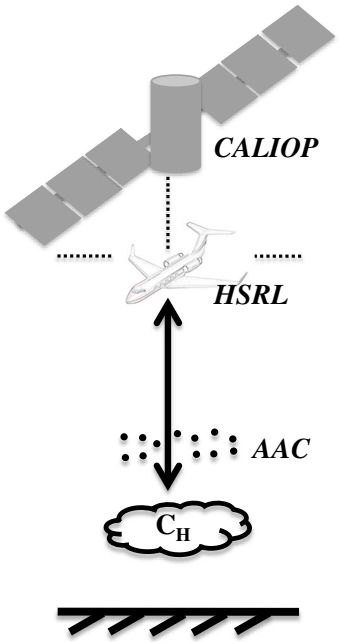

No cloud or aerosol above HSRL-airplane	Delete profile if aerosol and/ or cloud detected by CALIOP above HSRL-airplane
HSRL airplane	
CALIOP cloud-free AAC AOD	Delete lower part of profile if CALIOP σ_a not satisfying : • $-0.1<\sigma_a<1.25$ km^{-1} • σ_a QC=0,1,2,16,18,129* • $\lvert\delta(\sigma_a)x100/\sigma_a\rvert<400\%$ *with S_a between 20 and 80 sr
HSRL cloud-free AAC AOD	Select only HSRL $\sigma_a>0.01$ km^{-1} and delete profile if less than five $\sigma_a>0.01$ km^{-1} on vertical
Cloud top height *defined by HSRL for both HSRL and CALIOP AAC*	

Figure 1. Illustration of CALIOP and HSRL colocation and respective lidar-derived products used in the case of an aerosol-above-cloud (AAC) layer between the HSRL airplane and the target cloud top height C_H. The CALIOP profile products have a 5 km horizontal and 60 m vertical resolution, and the nearest HSRL profile products have a ~4/3 km horizontal and 30 m vertical resolution. Any of the paired CALIOP-HSRL profiles showing a difference in time greater than 30 min and/or a difference in location at the ground above 5 km were deleted from the data set. An "aerosol-free and cloud-free" filter is applied above the HSRL airplane. Specific quality criteria, a relative uncertainty upper threshold, and an interval range are applied to CALIOP extinction coefficients, and a lower threshold is applied on the HSRL extinction coefficients. The aerosol extinction coefficient and its uncertainty are, respectively, noted σ_a and $\delta(\sigma_a)$.

described the potential errors introduced in any of these quantities and found the 532 nm extinction systematic errors to be less than 0.01 km^{-1} for typical aerosol loading.

[8] The LaRC HSRL team also produces an aerosol classification scheme [*Burton et al*., 2012] that classifies the measurements into eight major types: ice, pure dust, dusty mix, maritime, polluted maritime, urban, fresh smoke, and smoke. The HSRL classification method uses four aerosol intensive variables (i.e., parameters that do not vary with aerosol amount): the aerosol depolarization ratio at 532 nm, the extinction-to-backscatter ratio at 532 nm, the backscatter color ratio, and the spectral ratio of depolarization ratios at 532 nm and 1064 nm. In this study, we are using the HSRL "cloud_top_height" parameter which is calculated using a convolution of the measured signal at 532 nm with a Haar wavelet to enhance edges [*Davis et al*., 2000], combined with an algorithm to set a flight-by-flight threshold for separating the generally sharper cloud edges from the less pronounced aerosol feature boundaries in each lidar profile [*Burton et al*., 2012].

2.2. Colocation of HSRL and CALIOP Aerosol-Above-Cloud

[9] Figure 1 illustrates the different products used in the colocation of HSRL and CALIOP profiles. Each CALIOP aerosol profile product (with a 5 km horizontal and 60 m vertical resolution) was colocated to the nearest HSRL profile in time and space (subset files with a ~4/3 km horizontal and 30 m vertical resolution). Any of these paired CALIOP-HSRL profiles showing a difference in time >30 min and/or a difference in location at the ground >5 km were deleted from the data set. We note that the relevance of a 30 min and 5 km spatiotemporal maximum separation between CALIOP and HSRL AOD depends on the aerosol variability from one environment to another [*Redemann et al*., 2006; *Shinozuka and Redemann*, 2011]. R. R. Rogers et al. (manuscript in preparation, 2014) have assessed how much the AOD changed as a function of time by matching locations on overlapping HSRL tracks of opposite directions within 2.5 km. Their analysis shows that the HSRL AOD values were well correlated in the Planetary Boundary Layer (PBL) ($R^2 > 0.9$) with up to 1.5 h separation (or roughly 555 km as the HSRL airplane usually flies at ~370 km/h). Since our colocation requirement is longer than 2.5 km (i.e., 5 km), it is important to note that the potential temporal and spatial mismatch between HSRL and CALIOP observations could have some effect on the AOD comparison presented in this study.

[10] As a first step, we define the uppermost cloud below the HSRL airplane (C_H in Figure 1), using the HSRL "cloud_top_height" parameter. This results in one C_H value for both CALIOP and HSRL AAC observations. Let us note that the HSRL team has performed a similar assessment of how much the HSRL cloud fraction changed as a function of time along the HSRL track. The cloud fraction correlation drops off much faster (after ~20–30 min) than the one for aerosols, leading to the conclusion that clouds are subject to more dynamical processes, giving rise to much greater spatial variability than aerosol. The CALIOP and HSRL AAC AOD values are then respectively defined as the integration of the CALIOP 5 km aerosol extinction profile and HSRL 4/3 km aerosol extinction profile from the height of the HSRL airplane (most frequently around 8 km) down to C_H. As described in Figure 1, any CALIOP extinction coefficients outside the −0.1 to 1.25 km^{-1} range at 532 nm and/or showing a relative extinction uncertainty value above 400% and/or not satisfying specific quality control criteria (points have to satisfy "Extinction_QC_flag_532" = 0, 1, 2, 16, 18 or 129; see http://www-calipso.larc.nasa.gov/resources/calipso_users_guide/data_summaries/layer/index.php#extinctionqc_532) were deleted from the analysis together with all underlying extinction coefficients in the profile. Because the CALIOP SNR is quite low, especially for daytime retrievals, small negative values can legitimately occur in the extinction retrieval. These values were retained to properly preserve the statistical scatter of solutions around the correct retrieval. Conversely, the HSRL profile was deleted when presenting less than five extinction coefficients on the vertical and an HSRL aerosol extinction coefficient was considered when >0.01 km^{-1} (HSRL extinction coefficients smaller than that value are consistent with observations of clean air). The AAC is defined as being cloud-free within and above the aerosol's altitude range and can be composed of different aerosol layers. The CALIOP AAC was assured cloud-free by selecting CALIOP profiles with the uppermost CALIOP cloud top heights lying at or below the corresponding HSRL cloud top height. The CALIOP extinction retrieval process works from the top of the atmosphere downward to the surface, correcting the signals from lower regions for the attenuation caused by higher features as this is retrieved [*Young and Vaughan*, 2009]. Any error in the CALIOP retrieval algorithm above the airplane will most likely propagate downward in the profile, and for this reason, we remove cases with high-altitude clouds (e.g., mostly cirrus clouds) or aerosol layers above the HSRL airplane using the CALIOP 5 km aerosol profile "atmospheric volume description" product. The "cloud-free and aerosol-free" filter above the HSRL airplane removes, respectively, 25% and 31% of the HSRL and CALIOP AAC cases. In addition, we emphasize that the determination of CALIOP AAC could appear more restrictive compared to the HSRL AAC because it requires additional quality control criteria on the aerosol extinction coefficient. Nonetheless, applying the filters on the extinction coefficients mentioned in the table of Figure 1 removes significantly less (6%) CALIOP AAC than HSRL AAC cases (27%). The 27% removed HSRL AAC cases correspond to a very low mean HSRL AAC AOD of $\sim 7 \times 10^{-4} \pm 4 \times 10^{-3}$. The combination of both "cloud-free and aerosol-free" and extinction coefficient filters removes, respectively, 35% and 43% of CALIOP and HSRL AAC cases. Finally, the HSRL aerosol classification product [*Burton et al*., 2012] provides information on the type of particle above cloud for each HSRL profile. The aerosol type we have selected for further analysis is set to be the most frequently observed over each specific cloud.

[11] Unless otherwise stated, the wavelength at which AOD values are given in this paper is 532 nm.

3. Results

3.1. Representativeness of Our HSRL-CALIOP Aerosol-Above-Cloud Data Set

[12] We have analyzed 1 year of CALIOP aerosol profile data (2007, 5 km horizontal resolution) between 60°S and 80°N in latitude (see Figure 2) to estimate the global frequency of AAC occurrence and the horizontal and vertical locations and optical depths of aerosols overlying the uppermost clouds at any altitude below 20 km. Our analyses of 12 months of CALIOP data (~7.9×10^5 AAC cases; see

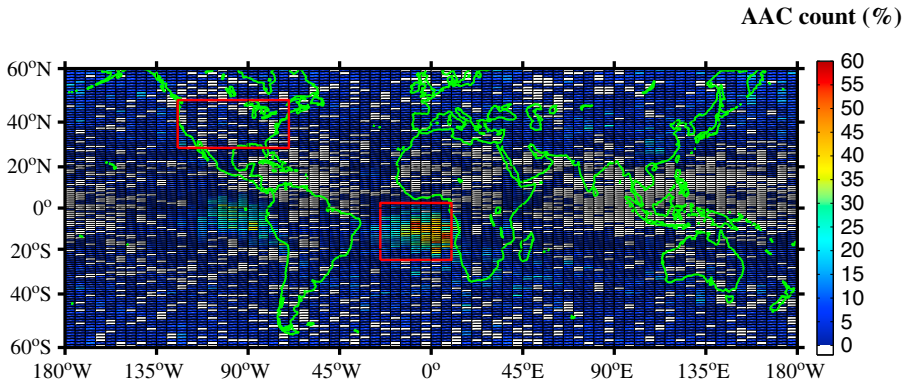

Figure 2. AAC occurrence according to CALIOP in October 2007 (use of CALIOP level 2 5 km aerosol daytime and nighttime profile products). The color bar is the percentage of CALIOP observations detected as AAC compared to the number of CALIOP observations detected as either "clear air," cloud, or aerosols in each 1° latitude × 5° longitude box. The pale gray cells show either no CALIOP data or CALIOP data without any AAC throughout the month of October 2007. The red boxes show the South East Atlantic (SEA) and the Northern American (NA) regions of Table 3.

Table 3) show that the AAC cases detected by CALIOP are, on average, located between an altitude of 3.8 ± 0.3 and 3.2 ± 0.3 km and appear to be separated by 0.7 km from an underlying cloud layer with cloud top altitude around 2.5 ± 0.3 km. According to CALIOP, the AAC cases show a global average midvisible (532 nm) AOD of 0.03 (above an uppermost cloud at any height below 20 km), which is appreciable when compared to a global MODIS background AOD of ~0.13–0.14 over ocean and 0.19 over land [*Remer et al.*, 2008] and a global average midvisible remote sensing composite AOD near 0.13 [*Kinne*, 2009].

[13] Although the HSRL measurements are highly accurate and best suited to evaluate CALIOP AAC, the collocated CALIOP-HSRL AAC data set of our study ($N = 171$ CALIOP and $N = 668$ HSRL AAC cases, Table 3) is sparse for two reasons. First, the design of the CALIOP airborne calibration validation experiments required the HSRL to fly in largely cloud-free conditions, and second, a majority of CALIOP-HSRL coincident tracks are located over land and not over the ocean where most of the AAC seems to reside. Indeed, a global climatological distribution of daytime low-altitude liquid water clouds derived from the International Satellite Cloud Climatology Project (ISCCP) shows a predominance of these clouds over oceanic areas where upwelling of cold water takes place along the western coasts of the continents [*Devasthale and Thomas*, 2011]. Aerosol-cloud overlaps are likely to occur when both natural and anthropogenic aerosols are transported over oceanic areas where low-level liquid clouds are common. This is the case, for example, offshore from the west coast of Central Africa where the area usually shows a marine boundary layer capped by homogeneous semipermanent stratocumulus [*Klein and Hartmann*, 1993; *Wood*, 2012]. Indeed, October 2007 (Figure 2) shows up to 60% CALIOP AAC occurrence offshore from Namibia, over the South East Atlantic (SEA). According to the MODIS Rapid Response Active Fire Detection map [*Justice et al.*, 2002] in October 2007, these aerosols are probably emitted by biomass burning. This is, by far, the main source of anthropogenic aerosols in the Southern Hemisphere.

[14] According to Table 3, the average AOD corresponding to the collocated CALIOP-HSRL AAC data set of our

Table 3. AAC Mean Midvisible (532 nm) AOD, Max AOD, Mean Altitude of Highest Aerosol Top, Mean Altitude of Lowest Aerosol Base, and Mean Altitude of Uppermost Cloud Top (i) Over the Globe (Between 60ºS and 80ºN in Latitude; See Figure 2 for October 2007), (ii) Over the South East Atlantic (SEA) ((30ºS,10ºN; 35ºW, 14ºE), Red Box on Figure 2), (iii) over Northern America (NA) ((12ºN,75ºN; 165ºW, 60ºW), Red Box on Figure 2), and (iv) Over the Locations (Mostly the U.S.) and During the 86 Flights of Table 1[a]

Aerosol Above Cloud	Lidar	Mean AOD	Max AOD	Mean Height Highest Aerosol Top (km)	Mean Height Lowest Aerosol Base (km)	Mean Height Uppermost Cloud Top (km)
Globe 2007	CALIOP ($N = 7.87E+05$)	0.03 ± 0.03	1.53	3.78 ± 0.31	3.20 ± 0.30	2.47 ± 0.30[b]
South East Atlantic 2007	CALIOP ($N = 6.90E+04$)	0.06 ± 0.04	1.11	3.49 ± 0.45	2.60 ± 0.52	1.82 ± 0.50[b]
North America 2007	CALIOP ($N = 1.09E+05$)	0.02 ± 0.01	0.43	4.14 ± 0.37	3.54 ± 0.34	2.61 ± 0.37[b]
Mostly U.S. 86 flights of Table 1	CALIOP ($N = 171$)	0.05 ± 0.06	0.37	2.92 ± 1.19	2.17 ± 0.97	1.91 ± 1.02[c]
	HSRL ($N = 668$)	0.04 ± 0.05	0.63	6.22 ± 0.26	2.36 ± 0.79	

[a]The AAC in case (i–iii) use 12 months of CALIOP 5 km day and nighttime aerosol profile products in 2007 and is defined as aerosol layer(s) above the uppermost-detected cloud below an altitude of 20 km; the list of filters in the "CALIOP cloud-free AAC AOD" row in the table of Figure 1 is applied to case (i–iv). The rest of the table in Figure 1 is applied to case (iv). The arithmetic averages in case (i–iii) are sums in each of the 1° × 5° bins of Figure 2, divided by the number of CALIOP AAC cases per bin during the 12 months. One averaged value and its corresponding standard deviation is then obtained by averaging all spatial bins. The maximum AOD value is the absolute maximum value over the region of interest.

[b]CALIOP-detected cloud below 20 km.

[c]HSRL-detected cloud below airplane.

Table 4. Total Number of (1) Coincident Profiles Below the HSRL Airplane (Line 1), (2) HSRL and/or CALIOP Profiles Showing Aerosol Observations Anywhere Between the HSRL Airplane and the Ground (Lines 2–4), (3) HSRL Profiles Recording Underlying Clouds (Line 5), and (4) Observed HSRL and/or CALIOP AAC Observations (Lines 6–8; See Figure 1 for Definition of AAC)[a]

Below the HSRL Airplane CALIOP and HSRL in the 5 km and/or 30 min Range	
Both HSRL and CALIOP profiles record aerosol, cloud, and/or clear air	2779
HSRL profiles record aerosol	2540
CALIOP profiles record aerosol	1673
Both HSRL and CALIOP profiles record aerosol	1488
HSRL profiles record cloud	993
HSRL profiles record AAC	668
CALIOP profiles record AAC	171
Both HSRL and CALIOP profiles record AAC	151

[a]All CALIOP-HSRL data are based on Table 1 with a 5 km 30 min maximum range between both lidars. Results are aerosol-free and cloud-free above the HSRL airplane, according to CALIOP.

study (i.e., 0.04–0.05) is slightly above the 2007 yearly average CALIOP AAC AOD over the globe (i.e., 0.03) and over North America (NA) (i.e., 0.02, red box on Figure 2). We find that March through May are the months of highest AAC occurrence in 2007 over NA, in agreement with *Devasthale and Thomas* [2011]. The average AOD corresponding to the collocated CALIOP-HSRL AAC data set of our study (i.e., 0.04–0.05) is also slightly above the March–May 2007 CALIOP AAC AOD average over NA (i.e., 0.03).

[15] Additional airborne HSRL data over areas of high AAC occurrence, similar to the region of SEA on Figure 2, would provide a drastic increase in the number of coincident CALIOP-HSRL data points and a wider range of AAC AOD values (i.e., higher maximum and average AAC AOD). According to Table 3, the average AOD corresponding to the collocated CALIOP-HSRL AAC data set of our study (i.e., 0.04–0.05) is lower than CALIOP AAC AOD over SEA for both the 2007 yearly average (i.e., 0.06) and the peak months of August–October 2007 (i.e., 0.08).

3.2. HSRL Versus CALIOP Aerosol-Above-Cloud

[16] Using the method described in section 2.2 and the colocated CALIOP-HSRL profiles of Table 1, we find a total of 2779 coincident CALIOP and HSRL profiles showing aerosol, cloud, and/or "clear air" observations below the HSRL airplane (Table 4). We note that those cases are cloud-free and aerosol-free above the HSRL airplane. Table 4 shows ~53% ($N = 1488$) of those 2779 profiles exhibiting coincident CALIOP and HSRL aerosol observations anywhere between the HSRL airplane and the ground. Furthermore, for ~36% ($N = 993$) of those 2779 profiles, the HSRL detects underlying clouds.

[17] When analyzing each lidar separately on the flight tracks of Table 1 (i.e., without considering aerosol detection by the other lidar), we find a total of 668 HSRL AAC cases (defined in section 2.2) compared to a total of 171 CALIOP AAC cases. Based on those 668 HSRL and 171 CALIOP observations (Tables 3 and 4), both instruments show a majority of AAC AOD values to be <0.1 with an average AOD of 0.04–0.05 ± 0.05–0.06 (similar to a global 2007 yearly CALIOP mean AAC AOD of 0.03 in Table 3) and a maximum value of 0.37 for CALIOP compared to 0.63 for HSRL. Moreover, the clouds underlying the AAC have an average top height of ~1.91 ± 1.02 km (compared to a global 2007 yearly CALIOP mean cloud top height for AAC of 2.47 ± 0.30 km in Table 3).

[18] Table 4 shows 668 (24% of the initial 2779) profiles exhibiting AAC cases according to HSRL, leading to the supposition that AAC should be expected to occur 24% of the time over our area and during our period of study. On another hand, Table 4 shows that 171 (6% of those 2779) profiles are recorded as AAC cases by CALIOP. According to Table 4, 151 profiles show coincident CALIOP and HSRL AAC cases. There are a few cases where CALIOP shows AAC observations and HSRL does not ($N = 20$). Among those 20 missing HSRL AAC cases, 9 of them were removed due to the filtering of the extinction coefficients (see table of Figure 1) and 11 of those cases were truly nonretrieved HSRL aerosol profiles. Although some sampling errors could be induced by the relative scarcity of boundary layer clouds in the CALIOP-HSRL data set and the imperfection of the temporal and spatial colocation between both lidars, our first assessment is that CALIOP detects the presence of AAC in only ~23% ($N = 151$ compared to 668) of the cases where the HSRL detects AAC. In other words, CALIOP detects no AAC in ~77% of the cases in which HSRL does. We explain this lack of CALIOP detection of AAC in ~77% of the cases mostly by the presence of faint aerosol layers below the CALIOP detection threshold (see section 3.3.2). Section 3.3 describes the potential sources of CALIOP errors in the AAC detection and retrieval with further details.

[19] The insert of Figure 3 shows the geographical location of the colocated HSRL and CALIOP AAC AOD observations ($N = 151$, in red) compared to all HSRL profiles exhibiting AAC cases ($N = 668$, in blue; see Table 4). With the exception of a few cases over Alaska ($N = 12$ during the Arctic Research of the Composition of the Troposphere from Aircraft and Satellites experiment), most of the AAC layers are found over the Eastern, Central, and South Central United States. The insert of Figure 3 also shows that CALIOP seems to better observe AAC in the Eastern and Southern US than in the Arctic and Canada. According to the distribution of aerosol type (Figure 3) using the HSRL classification scheme [*Burton et al.*, 2012], these 151 AAC cases are mostly composed of urban (~46%), dusty mix (~27%), and biomass burning smoke (~13%).

[20] The distribution of the AAC type according to CALIOP is fairly different from the one derived by the HSRL. According to CALIOP, the AAC cases are composed of a majority of polluted dust (~43%), smoke (~26%), and clean continental (11%). Section 3.3 investigates the comparison of AAC types from CALIOP and HSRL in further detail. Figure 4 shows the direct comparison ($N = 151$) between AAC AOD from CALIOP and HSRL. The dashed lines on both sides of the 1:1 line in Figure 4 represent a CALIOP AOD uncertainty envelope of ±40% (i.e., as given in *Winker et al.* [2009]). CALIOP shows little correlation with HSRL for combined day and night measurements ($R^2 = 0.27$). The lack of correlation remains similar, but the number of data points drops drastically when using only the nighttime colocated lidar

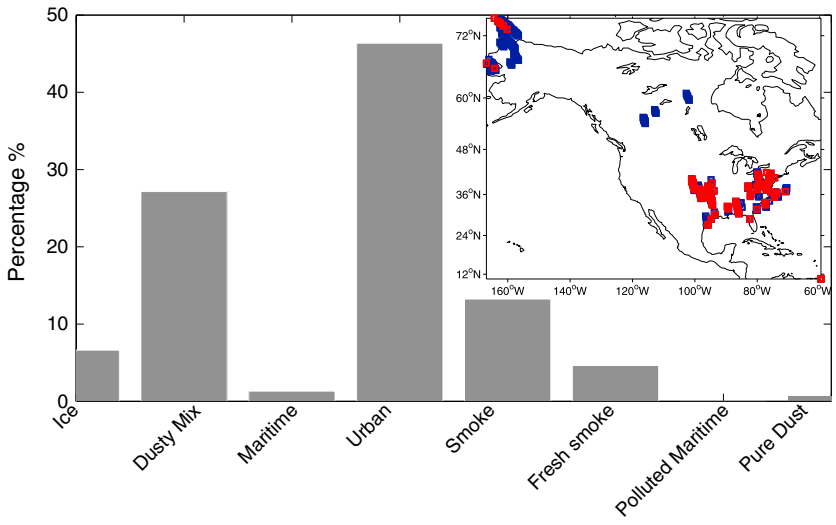

Figure 3. Feature type above cloud according to the HSRL classification algorithm [*Burton et al.*, 2012] for day and night HSRL-CALIOP colocated AAC cases with no clouds or aerosols above the HSRL airplane. The insert map shows the location of the corresponding AAC AOD retrievals (red, $N = 151$) compared to all HSRL profiles showing AAC cases (blue, $N = 668$; see Table 4).

measurements ($R^2 = 0.08$ and $N = 27$). We note that an extensive comparison of HSRL and CALIOP AOD in the absence of clouds is in preparation (R. R. Rogers et al., manuscript in preparation, 2014). This comparison finds that by day, CALIOP frequently does not detect thin aerosol layers with AOD < 0.1. In general, compared with the HSRL values, the CALIOP cloud-free layer AOD was biased high by less than 50% for AOD below 0.3 with higher errors for higher AOD.

[21] About 32% of the CALIOP-HSRL AOD data set ($N = 48$) of Figure 4 is within the ±40% envelope. Among the points outside the envelope (68%), 25% are above the +40% line (i.e., CALIOP overestimates HSRL) and 43% are below the −40% line (i.e., CALIOP underestimates HSRL). If the two data points exhibiting a CALIOP AOD above 0.3 on Figure 4 are removed from the analysis, the red regression line changes from an overall CALIOP overestimation of the HSRL AOD to being within the ±40% envelope. We emphasize that most of the AAC cases in our study show CALIOP and HSRL AOD values below 0.1 at 532 nm, and we observe a CALIOP underestimation of HSRL in a slight majority of cases. Further investigations of data points in the 0–0.1 CALIOP AAC AOD range on Figure 4 show low backscatter intensity, demonstrated by both the HSRL aerosol backscatter coefficient (majority below 4×10^{-4} km^{-1} sr^{-1}) and high horizontal averaging required by CALIOP for detection (80 or 20 km compared to 5 km for more strongly scattering layers). All other factors remaining equal, the aerosol backscatter intensity of a layer that can be detected only after horizontal averaging over 80 km is appreciably less than that of a layer requiring only 20 km or 5 km of horizontal averaging [e.g., *Vaughan et al.*, 2009, Figure 8]. This low feature backscatter intensity in most AAC cases points strongly to the presence of faint aerosol layers possibly below the CALIOP detection threshold and contributing to CALIOP "missing" a part of the AAC load. Section 3.3 lists and attempts to quantify the contribution of several factors to the accuracy of the standard version 3 CALIOP AAC retrieval. Section 3.4 further advances this study by applying an alternative CALIOP aerosol extinction retrieval method to the coincident CALIOP-HSRL data set of Figure 4.

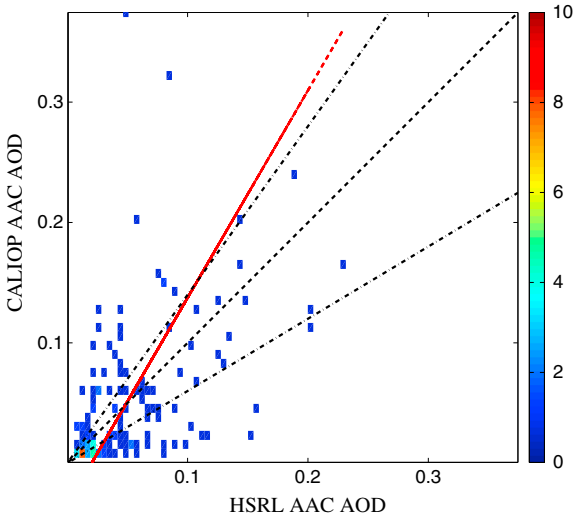

Figure 4. CALIOP versus HSRL AAC AOD at 532 nm with day and night measurements (red regression line: CALIOP AAC AOD = 1.72 ± 0.23 HSRL AAC AOD −0.03 ± 0.01, $R^2 = 0.27$, $N = 151$, RMSE = 0.07, and bias = 3.68×10^{-18}). The cloud underlying the aerosol is defined by HSRL. The profiles are cloud-free and aerosol-free above the HSRL airplane according to CALIOP. The color bar shows the percentage of points in each cell compared to the total number of coincident CALIOP-HSRL AAC cases ($N = 151$). The dashed lines represent CALIOP AAC AOD = HSRL AAC AOD ± 40% HSRL AAC AOD and 1:1 line. If we define the red line as $y_i = ax_i + b$, then RMSE = square root $((1/N - 2) \times \sum_i (y_i - ax_i - b)^2)$ and bias = $(1/N) \times \sum_i (y_i - ax_i - b)$.

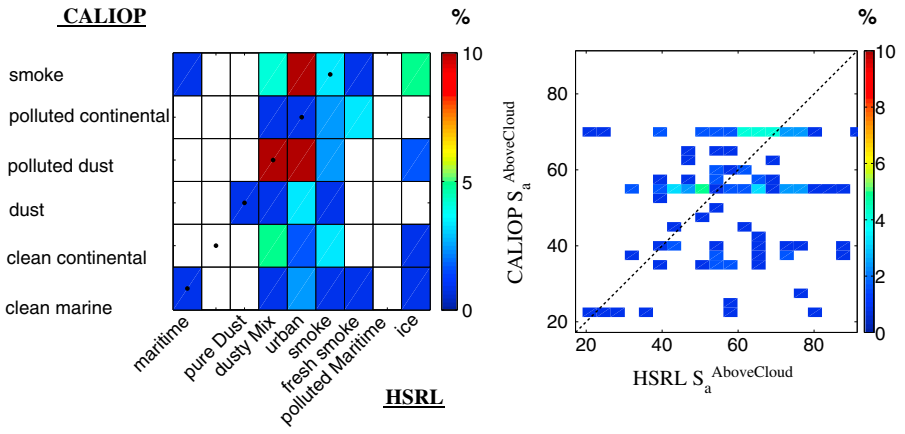

Figure 5. (left) CALIOP versus HSRL inferred aerosol types above clouds; dots show a priori matches (or close similarity) between CALIOP and HSRL aerosol types. (right) CALIOP versus HSRL $S_a^{AboveCloud}$ (see equation (1)). The color bar on each plot shows the percentage of points in each cell compared to the total number of coincident CALIOP-HSRL AAC cases.

3.3. Potential Errors in CALIOP Aerosol-Above-Cloud Detection and Classification

[22] Other than the calibration uncertainties in the CALIOP 532 nm channel (expected to have a bias no larger than ~3% according to *Rogers et al.* [2011]), we list the following potential impact factors on HSRL and CALIOP AAC detection efficiency and AOD retrieval: (i) a potential temporal and horizontal mismatch between CALIOP and HSRL observations (in the 30 min 5 km range, discussed in section 2.2), (ii) an aerosol type misclassification in the CALIOP retrieval algorithm, and (iii) a misdetection of the total or partial extent of the aerosol layer above cloud due to the presence of tenuous aerosol layers exhibiting backscatter coefficients below the CALIOP detection threshold. We speculate that the impact factor (i) would affect both lidar retrievals of AAC equally and would not induce any particular bias on one lidar observation or the other. Sections 3.3.1 and 3.3.2, respectively, attempt to quantify the impact of factors (ii) and (iii) on our CALIOP-HSRL AAC comparison study (data set of Figure 4).

3.3.1. Aerosol Type Misclassification

[23] A CALIOP overestimation or underestimation of HSRL AOD could be due to an incorrect CALIOP aerosol classification of the layer [*Omar et al.*, 2009]. First, the CALIOP misclassification of the aerosol layer can be caused by low CALIOP signal-to-noise ratio (SNR). CALIOP's SNR is lower than for typical ground-based or airborne lidars because the instrument is far from the atmosphere, the laser pulse energy is limited by the available electrical power, and the footprint is moving across the Earth's surface at nearly 7 km/s. The CALIOP SNR can also be further decreased in the presence of a thick aerosol layer overlying clouds (i.e., the signal is attenuated) or due to sunlight reflected from clouds (i.e., the noise is increased). The second reason for a potential CALIOP misclassification of the aerosol comes from the fact that CALIOP necessarily uses loading-dependent lidar measurements and information that are only indirectly related to aerosol type (volume depolarization, attenuated backscatter, aerosol location, height, and surface type), rather than the exclusively intensive aerosol properties used by the HSRL aerosol classification [*Burton et al.*, 2012]. *Burton et al.* [2013] use HSRL-1 observations as inputs to the CALIOP classification scheme and conclude that it is not primarily the increased SNR that allows for more accurate aerosol classification from the HSRL-1 measurements but instead the increased information content in the form of aerosol intensive parameters that give direct insight into aerosol type.

[24] A comparison study by *Mielonen et al.* [2009] between aerosol types derived from CALIOP (previous version 2.01) and coincident AEronet RObotic NETwork (AERONET) stations (the AERONET aerosol types were categorized by single scattering albedo and Angstrom exponent values) shows 70% of both AERONET and CALIOP aerosol types in agreement, with the best agreement achieved for the CALIOP "dust" and "polluted dust" types. However, a comparison study between the HSRL and the CALIOP aerosol classification by *Burton et al.* [2013] shows relatively poor agreement for polluted dust (i.e., 35% of CALIOP agrees with the HSRL-1 results) and smoke (13%), compared to marine (62%), polluted continental (54%), and desert dust (80%).

[25] Figure 5 (left) compares CALIOP and HSRL aerosol types for all AAC cases of Figure 4. Assuming HSRL classifications are true, CALIOP seems to mostly misclassify four aerosol types (smoke, polluted continental, dust, and clean marine) and to classify more correctly the aerosol type polluted dust (i.e., the paired polluted dust and "dusty mix" show the highest coincident CALIOP-HSRL data percentage both in the x and y axes of Figure 5 (left)) for the data set analyzed in this study. We note that the CALIOP polluted dust and the HSRL "dusty mix" are not identical aerosol types as the former is specifically modeled as a mixture of dust and smoke and the latter is a mix of dust and any other aerosol. Nothing can be said about CALIOP "clean continental" as HSRL presents no equivalent aerosol type. Let us note that the ~77% cases of Table 4 where CALIOP detects no AAC when HSRL does are mostly composed of urban (~44%), dusty mix (22%), and smoke (21%) according to the HSRL classification scheme.

[26] A CALIOP misclassification will likely result in an incorrect inference of the appropriate CALIOP lidar ratio (S_a). In addition to the natural variabilities of the S_a given in Table 2, an erroneous S_a could be assumed even when the aerosol type is correctly defined. For example, *Schuster et al.* [2012] used a coincident CALIOP-AERONET data set over

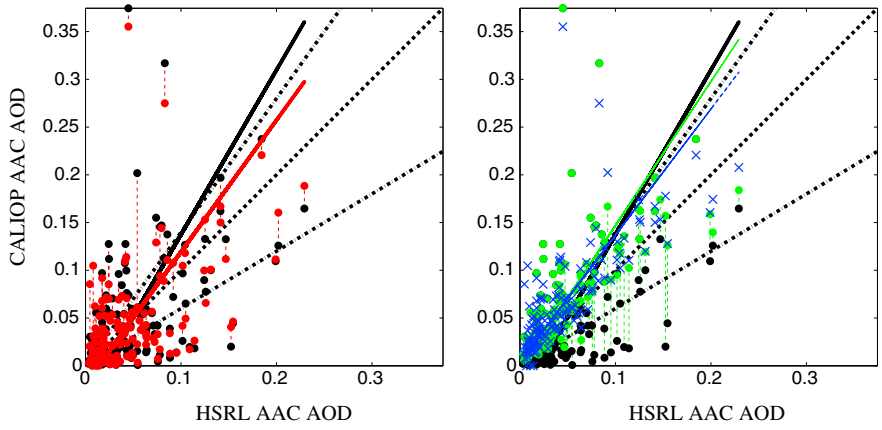

CALIOP standard or corrected versus HSRL AAC AOD	AAC AOD	AAC AOD	AAC AOD	AAC AOD^{Sacor,Detcor}
R^2	0.27	0.30	0.52	0.57
Slope	1.72 ± 0.23	1.38 ± 0.17	1.51 ± 0.12	1.32 ± 0.09
Offset	-0.04 ± 0.01	-0.02 ± 0.01	0.00 ± 0.01	0.00 ± 0.00
Number of points in ±40% envelope	32%	38%	54%	49%
RMS difference CALIOP-HSRL	0.052	0.047	0.046	0.041
RMS change from initial CALIOP AAC AOD		0.022	0.034	0.052
Reduction in RMS difference as % of mean HSRL AAC AOD (0.047)		-11%	-14%	-24%

-standard
-corrected for S_a
-corrected for detection
-corrected for both above

Figure 6. (top left) HSRL AAC AOD versus CALIOP standard AAC AOD (black) and CALIOP corrected for erroneous S_a, AAC AOD^{Sacor} (red) and (top right) HSRL AAC AOD versus CALIOP standard AAC AOD (black), CALIOP corrected for misdetection underneath the 1:1 line, AAC AOD^{Detcor} (green) and CALIOP corrected for both erroneous S_a and misdetection, AAC AOD^{Sacor,Detcor} (blue); (bottom) correlation coefficient, slope, offset, standard deviation, percentage of points in the ±40% envelope around the 1:1 line, RMS difference between CALIOP and HSRL, RMS change from the initial CALIOP AAC AOD data points, and reduction in the RMS difference as a percentage of the mean HSRL AAC AOD (0.047 at 532 nm).

147 AERONET stations to demonstrate that the lidar ratio for the CALIOP global dust model (40 sr) often underestimates the local lidar ratio. For the purpose of comparing CALIOP and HSRL S_a, we have integrated the S_a vertically from the aircraft down to the cloud. In our study, the CALIOP integrated S_a for each AAC is noted $S_a^{AboveCloud}$ and is the ratio of the integrated aerosol extinction coefficient profile $\sigma_a(z)$ by the integrated aerosol backscatter coefficient profile $\beta_a(z)$ as in equation (1):

$$S_a^{AboveCloud} = \frac{\int_{HSRLairplane}^{C_H} \sigma_a(z)dz'}{\int_{HSRLairplane}^{C_H} \beta_a(z)dz'} \quad (1)$$

where C_H is the underlying HSRL-derived cloud top height (see Figure 1). Figure 5 (right) shows no correlation between CALIOP and HSRL $S_a^{AboveCloud}$ ($R^2 = 0.038$, CALIOP $S_a^{AboveCloud} = 0.77 \pm 0.35 \times$ HSRL $S_a^{AboveCloud} + 10.39 \pm 20$, and $N = 122$). Whether due to incorrect typing or inaccurate lidar ratio modeling, the CALIOP lidar ratio assignments are clearly erroneous, with, for example, numerous data points showing a CALIOP $S_a^{AboveCloud}$ value of ~70 sr (corresponding to the CALIOP biomass burning "smoke" aerosol type; see Table 2) with a large range of corresponding HSRL $S_a^{AboveCloud}$ from ~17 to 91 sr. In the following section of this study, we correct CALIOP AAC AOD using equation (4) for a potentially wrong assumption of the CALIOP $S_a^{AboveCloud}$. We introduce equations (2) and (3) to explain equation (4). It was shown in *Platt* [1973] that the CALIOP aerosol layer-integrated attenuated backscatter (γ_a', sr^{-1}) can be written as follows:

$$\gamma_a' = \int_{top}^{base} \beta_a'(r)dr = \frac{1 - T_a^{2\eta_a}}{2\eta_a S_a} \quad (2)$$

where β_a' is the aerosol attenuated backscatter coefficient at range r (km^{-1} sr^{-1}), T_a is the two-way transmittance due to aerosols, and η_a is the aerosol multiple scattering factor. Assuming multiple scattering effects are negligible (i.e., $\eta_a = 1$), T_a^2 is function of τ_a, the aerosol optical depth as follows:

$$T_a^2 = \exp(-2\tau_a) \quad (3)$$

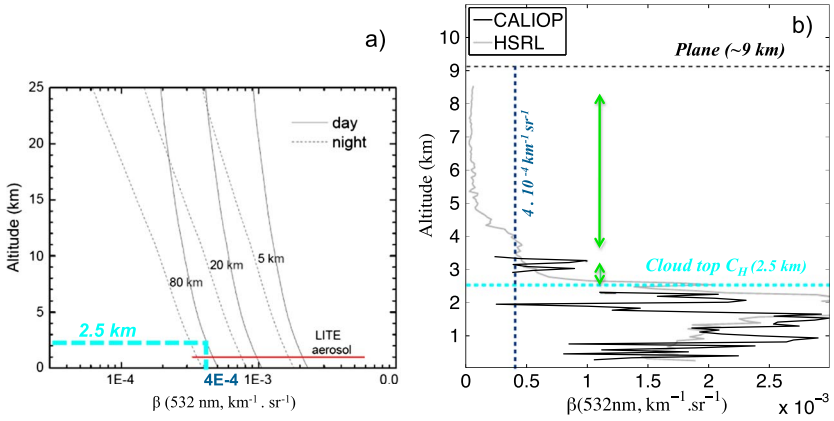

Figure 7. (a) Detection sensitivity of CALIOP 532 nm channel on profiles horizontally averaged to 5, 20, and 80 km (reproduced from *Vaughan et al*. [2005]); (b) example of two coincident CALIOP (black) and HSRL (grey) aerosol daytime backscatter profiles on 2 August 2006 showing a difference of CALIOP-HSRL AAC AOD of −80% (CALIOP AAC AOD of 0.01 compared to 0.05 for HSRL at 532 nm) with a CALIOP horizontal averaging of 80 km. The green vertical arrow describes the CALIOP portion of "missing" AOD between the HSRL airplane and the top of the cloud due to faint aerosols below the CALIOP detection threshold (arbitrary threshold of 4×10^{-4} km^{-1} sr^{-1}, blue dashed vertical line on Figure 7a).

[27] This leads to

$$\gamma_a' = \frac{1 - \exp(-2\tau_a)}{2S_a} \text{ and } \quad \tau_a = -0.5 \times \ln\left(1 - 2\gamma_a' S_a\right) \quad (4)$$

[28] We have corrected the CALIOP AAC AOD values of Figure 4 by using equation (4) with γ_a' from CALIOP and, for S_a, the integrated HSRL $S_a^{AboveCloud}$ (equation (1)). We call the result AAC AOD^{Sacor}. Figure 6 (top left) shows the comparison between the paired (CALIOP AAC AOD; HSRL AAC AOD) (black) and (CALIOP AAC AOD^{Sacor}; HSRL AAC AOD) (red) values. A light red vertical dashed line links each red and black point. One result of correcting CALIOP with the accurate HSRL S_a is an increase in the fraction of red (corrected) points within the ±40% envelope as compared to the fraction for black (uncorrected) points (38% for red compared to 32% for black); however, this increase is relatively slight. Also, the red slope is closer to 1 (1.4 compared to 1.7), and the correlation coefficients are similar ($R^2 \sim 0.3$). Because the improvements are minor, we conclude from Figure 6 that an erroneous modeled CALIOP S_a is not the dominant source of error in the CALIOP overestimation or underestimation of the HSRL AAC AOD.

3.3.2. Misdetection of Total or Partial Vertical Extent of the Aerosol Layer

[29] The HSRL provides a direct and unambiguous retrieval of extinction throughout each measured profile without the assumption of S_a. CALIPSO, on the other hand, attempts to retrieve aerosol extinction coefficients (and hence AOD) only in those regions where the CALIOP layer detection and classification schemes identify the presence of aerosol layers. As a consequence, aerosols with backscatter intensities below the CALIOP layer detection threshold will not contribute to the CALIOP AOD estimates. When such faint aerosol layers are present, the CALIOP-retrieved AOD is likely to underestimate the AOD measured by HSRL. Figure 7a shows theoretical calculations of profiles of the minimum detectable CALIOP backscatter coefficient at 532 nm, for day or nighttime measurements and with different amounts of horizontal averaging for detection [*Vaughan et al*., 2005]. CALIOP's detection sensitivity increases by averaging to 20 km or 80 km resolution, increases as a function of increasing altitude (because molecular density decreases as a function of increasing altitude), and is higher for nighttime compared to daytime measurements (because nighttime SNR is much better than daytime SNR). The minimum daytime or nighttime CALIOP threshold to detect aerosols at an altitude of ~2–3 km is around ~2–4 × 10^{-4} km^{-1} sr^{-1} (with the highest horizontal averaging of 80 km).

[30] Table 4 shows 517 records of HSRL AAC without coincident CALIOP AAC (i.e., 668–151). Those missing CALIOP AAC cases show a very small HSRL AOD (mean of 0.04 ± 0.06 and median of 0.02 at 532 nm). More important from a CALIOP detection perspective, the HSRL aerosol backscatter coefficients for the AAC cases are also quite small, with a mean value of $1 \times 10^{-4} \pm 5 \times 10^{-4}$ km^{-1} sr^{-1}, a median value of 5×10^{-5} km^{-1} sr^{-1}, and ~79% of the points lying below 2×10^{-4} km^{-1} sr^{-1} (i.e., below the predicted CALIOP 80 km detection threshold).

[31] These findings strongly suggest that the tenuous nature of the aerosols above clouds is most likely the reason why CALIOP detects no AAC when HSRL does in ~77% of cases (Table 4).

[32] Moreover, even when CALIOP detects AAC cases, the amount of CALIOP AOD could very well be underestimated. Because CALIOP retrieves AOD only in those regions where aerosol layers are detected, when only some fraction of an aerosol layer is above the CALIOP detection threshold, the AOD for that region will almost certainly be underestimated. Figure 7b is an example of CALIOP underestimation of the HSRL aerosol backscatter profile below the HSRL airplane and above the underlying cloud (top measured by HSRL at ~2.5 km). The difference between CALIOP and HSRL AAC AOD on Figure 7b is −80% (CALIOP AAC AOD of 0.01 compared to 0.05 for HSRL at 532 nm). CALIOP (black profile) starts measuring an aerosol feature at an altitude near 3.5 km, whereas the HSRL profile starts detecting aerosols right below the HSRL airplane (grey profile). The missing

Table 5. Filters Needed to Select Specific Low Opaque Clouds in Order to Perform the Alternate CALIOP DR Aerosol Extinction Retrieval[a]

	Low Opaque Water Clouds for DR AAC Retrieval [*Chand et al*., 2008]
1	CALIOP CAD score ≥ 90 and $\neq 103,104$, and 105
2	CALIOP opacity flag = 1
3	CALIOP layer averaging = 5 km
4	CALIOP inverse of relative uncertainty on γ'_{water}, δ'_{water}, and $\chi'_{water} > 2$
5	CALIOP cloud top altitude ≤ 3 km
6	CALIOP ice/water phase is water (with high QA)
7	CALIOP $\gamma'_{water} > 0.04\ sr^{-1}$

[a]The γ'_{water} is the 532 nm liquid water cloud layer integrated attenuated backscatter, δ'_{water} is the layer integrated attenuated volume depolarization ratio, and χ'_{water} is the 1064/532 nm layer integrated attenuated total color ratio.

CALIOP aerosol (green vertical arrow on Figure 7) shows very low HSRL aerosol backscatter coefficients, mostly below the empirically determined detection threshold of $4 \times 10^{-4}\ km^{-1}\ sr^{-1}$ for CALIOP daytime measurements (vertical blue dashed line on Figure 7b, part of the CALIPSO documentation).

[33] In this section of the study, we have corrected the CALIOP standard AAC AOD data points that reside below the 1:1 line of Figure 4 for the missing portion of the profile (vertical green arrow on Figure 7, AAC AOD^{Detcor} in green on Figure 6 (top right)). The added missing portion is the vertical integration of the HSRL extinction coefficients that have no corresponding valid CALIOP extinction coefficients between the HSRL airplane and the cloud top height. We note that we account for the CALIOP misdetection failure in a very specific way; i.e., by using the HSRL extinction coefficients in the missing regions and not by using the optical depths that CALIOP would have computed using the CALIOP attenuated backscatter measurements in those same regions.

[34] Figure 6 (top right) shows a significant increase of the percentage of green data points (i.e., accounting for CALIOP detection failure) in the ±40% envelope and a higher correlation coefficient than for the red data points (respectively 54% compared to 32% and $R^2 \sim 0.5$ compared to $R^2 \sim 0.3$). Figure 6 also shows CALIOP AAC AOD corrected for both the aerosol-type misclassification (section 3.3.1) and the aerosol misdetection (noted AAC $AOD^{Sacor,Detcor}$ in blue). The correlation coefficient reaches $R^2 \sim 0.6$ and 49% of the blue data points remain within the ±40% envelope. The bottom three rows of the table in Figure 6 provide further results comparing the two corrections (for CALIOP aerosol-type misclassification and for CALIOP misdetection of the aerosol vertical extent). These comparisons show that overall, the impact of the second correction (i.e., for CALIOP misdetection of aerosol vertical extent) is both larger than the first (for CALIOP aerosol-type misclassification) and more successful in reducing CALIOP-HSRL differences in AAC AOD. Specifically, the second correction produces a slightly smaller RMS difference between CALIOP and HSRL AAC AOD (0.046 versus 0.047) and it produces a larger RMS change from the initial CALIOP AAC AOD (0.034 versus 0.022). The reduction in RMS CALIOP-HSRL difference, measured as a percentage of the mean HSRL AAC AOD of 0.047, is 14% for the second correction, compared to 11% for the first. Let us note that adding the "missing" HSRL extinction coefficients made the corrected CALIOP AAC AOD^{Detcor} larger than the HSRL AOD in 72% of the cases (70 points above the 1:1 line compared to 97 points initially below the 1:1 CALIOP-HSRL AAC AOD line). The latter seems to be the reason for an RMS difference smaller than expected between HSRL and CALIOP AAC AOD^{Detcor}. Applying both corrections (rightmost column) induces a relative reduction in RMS differences of 24%.

[35] We conclude that CALIOP's lack of detection above the cloud top height has more impact on the HSRL and CALIOP AAC AOD difference than an erroneous CALIOP S_a assumption. We attribute the remaining impact on the differences between HSRL and CALIOP AAC AOD to spatiotemporal collocation between both instruments (see section 2.2).

3.4. CALIOP Alternate Aerosol-Above-Cloud AOD

[36] We have observed (section 3.2) an overall poor correlation between HSRL and CALIOP standard $\tau_a^{AboveCloud}$ retrievals ($R^2 = 0.27$ and $N = 151$). Recall that CALIOP's standard AOD retrieval (denoted $CALIOP_{stan}$) requires, in most cases, the use of a modeled extinction-to-backscatter ratio derived from an inference of aerosol type. *Hu et al*. [2007a] and *Chand et al*. [2008] introduce alternative retrieval methods that use liquid water clouds as targets of known reflectivity under the aerosol layer to be retrieved. Because such "constrained retrievals" do not require knowledge of a lidar ratio, they tend to be much more accurate [*Young and Vaughan*, 2009]. Our purpose in this section is to apply an alternate CALIOP retrieval to the HSRL-CALIOP colocated AAC AOD values of Table 1. We then investigate the agreement of the CALIOP alternative AAC AOD values with both $CALIOP_{stan}$ and HSRL AAC AOD retrievals.

[37] Using the technique described by *Chand et al*. [2008], AOD and extinction Ångstrom exponent can be deduced directly from aerosol effects on light transmission. This technique, based on measurements of water cloud depolarization ratio (DR) [*Hu et al*., 2007a] at 532 nm, requires opaque clouds and retrieves AAC optical depth regardless of the nature of the overlying material. The opaque liquid water clouds used for the DR technique are selected using the seven filters of Table 5 applied to the CALIOP 5 km cloud layer products.

[38] Following equation (3), the CALIOP AAC AOD using the DR method (noted AAC AOD^{DR}) can be written as follows:

$$\text{AAC} \quad \text{AOD}^{\text{DR}} = -\frac{1}{2}\ln T_a^2 \tag{5}$$

[39] Maintaining the earlier assumption that aerosol multiple scattering effects can be neglected, the two-way transmittance for an aerosol layer overlying an opaque water cloud can be determined using

$$T^2 = \frac{\gamma'_{water,SS}}{\gamma'_{water,SS,unobs.}} \tag{6}$$

where $\gamma'_{water,SS}$ and $\gamma'_{water,SS,unobs.}$ are the obstructed and unobstructed (i.e., if the cloud were viewed by CALIOP through an otherwise clear atmosphere with negligible nonmolecular attenuation) single scattering value of the layer-integrated attenuated backscatter for an opaque water cloud [*Hu et al*., 2007a]. Moreover,

$$\gamma'_{water,SS} = \gamma'_{water} \times \eta_{water} \tag{7}$$

and

Table 6. Standard and Alternative AAC AOD[a]

Name	Retrieval/Calculation	Coincident CALIOP-HSRL
AAC AOD	Standard CALIOP retrieval [*Winker et al*., 2009]	151
AAC $AOD^{DR,theo}$	Equation (9) with $\gamma'_{water,SS,unobs.} = 0.0263$	12
AAC $AOD^{DR,exp}$	Equation (9) with $\gamma'_{water,SS,unobs.}$ measured and averaged over the region	12

[a]The last column shows the number of coincident CALIOP and HSRL day and night AAC observations.

$$\eta_{water} = \left(\frac{1-\delta'_{water}}{1+\delta'_{water}}\right)^2 \quad (8)$$

where η_{water} is the layer effective multiple scattering factor and δ'_{water} is the layer-integrated volume depolarization ratio of the water cloud [*Hu et al*., 2007b]. Rearranging equation (5), through (8), we obtain

$$\text{AAC} \quad AOD^{DR} = -\frac{1}{2}\ln\left(\left(\frac{\gamma'_{water}}{\gamma'_{water,unobs.}}\right)\left(\frac{1-\delta'_{water}}{1+\delta'_{water}}\right)^2\left(\frac{1+\delta'_{water,unobs.}}{1-\delta'_{water,unobs.}}\right)^2\right) \quad (9)$$

[40] Table 6 describes two ways of computing AAC AOD^{DR} (equation (9)). The first of these, denoted AAC $AOD^{DR,theo}$, is derived using theoretical values. For measurements of opaque layers unaffected by multiple scattering, $\gamma'_{water,SS,unobs.} = 1/2S_{water}$, where S_{water} is the layer extinction-to-backscatter ratio [*Platt et al*., 1999]. For water clouds with droplet sizes smaller than 50 μm, Mie calculations have shown that S_{water} has a value very close to 19 sr [*Pinnick et al*., 1983; *O'Connor et al*., 2004; *Hu et al*., 2006], and thus, a theoretical calculation of the single scattering layer integrated attenuated backscatter would be $\gamma'_{water,SS,unobs.} = 1/(2 \times 19) = 0.0263$. The second DR method calculation, denoted AAC $AOD^{DR,exp}$, uses empirically determined values of $\gamma'_{water,SS,unobs.}$ According to *Hu et al*. [2007a], estimates of $\gamma'_{water,SS,unobs.}$ can be obtained from measurements of water clouds that have similar cloud top heights and microphysical properties but are embedded in clear air. Estimates of $\gamma'_{water,unobs.}$ are obtained directly from the attenuated backscatter data. Similarly, estimates of the layer-effective multiple scattering factor η can also be obtained directly from the volume depolarization measurements using equation (8). Then following equation (7), $\gamma'_{water,SS,unobs.}$ is simply the product of η_{water} and $\gamma'_{water,unobs.}$.

[41] The first step is to use the seven criteria of Table 5 to select specific low opaque water clouds in our data set of Table 1 in order to compute the alternative CALIOP DR aerosol extinction retrievals. The resulting low opaque water clouds ($N = 217$) above which a CALIOP DR retrieval is possible show 157 overlying AAC cases according to HSRL with no aerosol or clouds above the HSRL airplane according to CALIOP. Among those 157 HSRL AAC cases, only 12 clouds show overlying aerosols detected by both CALIOP and HSRL (Table 6). Those 12 cases are located roughly above the eastern part of the United States (longitudes between −102°W and 80°W) and are only from four different flight segments (25 June 2006, 26 June 2007, 1 February 2008, and 5 June 2009). The extreme scarcity of the data set ($N = 12$) is due to (1) the few CALIOP low opaque water clouds in our data set and (2) the lack of CALIOP AAC detection above those clouds. Recall that the HSRL validation flights were specifically designed to avoid cloud contaminated time periods and flight paths (see section 3.1). In addition, most low opaque liquid water clouds reside over the ocean (especially over the tropics), far from our region of study [*Devasthale and Thomas*, 2011].

[42] The next step is to assess the averaged $\gamma'_{water,SS,unobs.}$ value of a significant sample of CALIOP unobstructed low opaque water clouds over the region of interest. The CALIOP unobstructed clouds were defined as located between −102°W and 80°W in longitude and presenting no aerosol or cloud above the HSRL airplane and above the specific target cloud (i.e., the target cloud is the only layer in the total atmospheric column). We find an empirical averaged value of $0.0225\ sr^{-1}$ for $\gamma'_{water,SS,unobs.}$ (using 85 nonobstructed low opaque water clouds satisfying the criteria of Table 5). This empirical value corresponds to a cloud lidar ratio of ~22 sr, which might be too high for a low opaque water cloud [*Pinnick et al*., 1983; *Hu et al*., 2006]. On the other hand, AAC $AOD^{DR,theo}$ was computed with an assumed theoretical value of $0.0263\ sr^{-1}$ for $\gamma'_{water,SS,unobs.}$ (corresponds to a cloud lidar ratio of ~19 sr).

[43] Figure 8 presents the computed alternative AAC AOD^{DR} values for the 12 coincident AAC cases of Table 6. According to *Chand et al*. [2008], the minimum AAC AOD^{DR} that can be detected with 99% confidence is around 0.12 during the day (dashed horizontal black line on Figure 8) and 0.10 at night. The HSRL classifies most of the 12 AAC cases as smoke aerosols and the only coincident CALIOP (standard and alternate), and HSRL AAC AOD value above the dashed line is classified as "urban" aerosol by HSRL on the *x* axis.

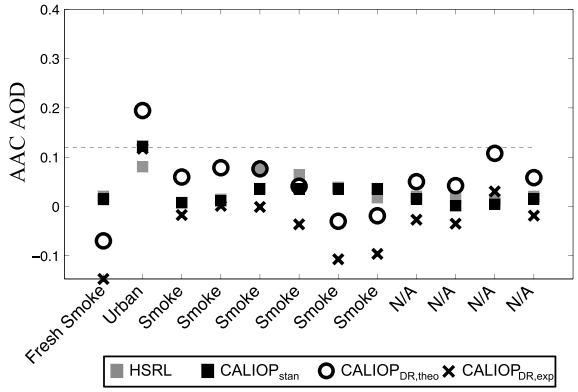

Figure 8. AOD values at 532 nm retrieved by HSRL (grey squares), $CALIOP_{stan}$ (black squares), $CALIOP_{DR,theo}$ ($\gamma'_{water,SS,unobs.} = 0.0263\ sr^{-1}$, black circles), and $CALIOP_{DR,exp}$ ($\gamma'_{water,SS,unobs.} = 0.0225\ sr^{-1}$, black crosses). All AAC AOD are (i) aerosol-free and cloud-free above the HRSL airplane according to CALIOP and (ii) overlying low opaque water clouds according to CALIOP and satisfying the criteria of Table 5. Note that we are showing all $CALIOP_{DR}$ AAC AOD points even if they lie below the daytime DR 99% confidence limit of 0.12 (horizontal dashed line).

[44] Although we observe some discrepancies between HSRL (grey squares), $CALIOP_{stan}$ (black squares), $CALIOP_{DR,theo}$ (black circles), and $CALIOP_{DR,exp}$ (black crosses), they remain fairly small and are contained below ~0.18 in AOD. There is a clear lack of data to push the analysis any further.

[45] Finally, we have analyzed the cases where only HSRL and $CALIOP_{DR}$ detect aerosol above low opaque water clouds satisfying the criteria of Table 5 (i.e., the CALIOP standard algorithm does not detect any AAC cases). For these cases ($N = 145$), we observe a lack of agreement between CALIOP AAC $AOD^{DR,theo}$ and HSRL AAC AOD ($R^2 = 0.38$; CALIOP AAC $AOD^{DR,theo} = 1.55 \pm 0.16$ HSRL AAC AOD + 0.03 ± 0.01, $N = 145$). However, it is important to note that 98% of those 145 cases record an HSRL AAC AOD below 0.12 (i.e., the 99% AOD confidence level for the DR method during the day according to *Chand et al*. [2008]). The respective HSRL and CALIOP DR average AAC AOD for those 145 cases are 0.04 ± 0.04 and 0.09 ± 0.05. The aerosol-free and cloud-free filter we impose above the HSRL airplane helps reduce any aerosol attenuation between CALIOP and the HSRL airplane altitude that would be included in the CALIOP DR AOD measurements but not in the HSRL measurements. In consequence, the larger CALIOP mean DR AAC AOD value of 0.09 cannot entirely be explained by the fact that the CALIOP DR method is based on the aerosol attenuation of the transmission through the entire atmospheric column (i.e., from the lidar at ~710 km down to the underlying cloud) compared to the integration of the extinction coefficient profile from the airplane down to the cloud in the case of the HSRL.

[46] In the end, we are in need of more suborbital field campaigns, especially over regions of the world showing high frequency of occurrence of AAC (e.g., the SEA region of section 3.1) together with low opaque clouds, in order to accurately evaluate $CALIOP_{DR}$, and $CALIOP_{stan}$ AAC AOD.

4. Conclusion

[47] We have used 86 suborbital HSRL flights to assess the CALIOP standard AAC detection and retrieval capability. First of all, we have analyzed CALIOP's ability to detect any (i.e., even the slightest) aerosol amount above cloud. We find that CALIOP detects AAC in ~23% of the cases in which it is observed by HSRL. The reason for a CALIOP underestimation of the AAC occurrence is that (i) as demonstrated in our study and consistent with published expectations, for small optical depths less than ~0.02, the standard CALIOP retrieval algorithm substantially underestimates the occurrence frequency of AAC and (ii) in our study (i.e., mostly over the continental US), a majority of the AAC AOD values lie below 0.1 with an average HSRL AAC AOD of ~0.04 ± 0.05. The latter is fairly similar to the 2007 yearly mean CALIOP AAC AOD over the globe or the March–May 2007 mean CALIOP AAC AOD over the North American region. These findings could have significant implications for studies that use CALIOP to determine the global horizontal and vertical location, type, amount, and optical and radiative properties of aerosols above clouds. We recommend caution when using AAC estimates obtained directly from the standard CALIPSO data products as it could lead to a global underestimation of the AAC occurrence. Furthermore, aerosols recording low AOD values (such as the AAC cases not observed by CALIOP) can still have a consequent radiative forcing effect as the latter depend on the underlying cloud cover (i.e., *Chand et al*. [2009]) show that smoke aerosols have a net warming effect that increases approximately linearly with cloud fraction) and the overlying aerosol absorption properties (function of the aerosol chemical composition, the aerosol vertical profile relative to cloud height, and the surface albedo of the underlying cloud).

[48] Second, we have assessed CALIOP's ability to successfully detect and retrieve the total amount of AAC (i.e., compared to HSRL). With the exception of a few cases over Alaska, most of the coincident CALIOP-HSRL AAC cases ($N = 151$) are found over the Eastern, Central, and South Central United States. According to the HSRL classification scheme, these AAC cases are mostly composed of urban (~46%), dusty mix (~27%), and biomass burning smoke (~13%). CALIOP shows essentially no agreement with HSRL for combined day and night AAC AOD measurements ($R^2 = 0.27$) and ~68% of the CALIOP AAC AOD values are outside the ±40% envelope of the CALIOP = HSRL line. The nondetection or underestimation of AAC AOD (i.e., the total number of aerosol layers or specific tenuous aerosol layers above each cloud) is mostly due to tenuous aerosol layers with backscatter coefficients below the CALIOP detection threshold. A minority of the discrepancy seems to be due to a CALIOP type misclassification or an error in the CALIOP modeled S_a. Compared to an erroneous S_a assumption, correcting for the CALIOP misdetection of aerosol vertical extent produces a larger RMS change from the initial CALIOP AAC AOD, a smaller RMS difference between CALIOP and HSRL AAC AOD, and a bigger reduction in RMS CALIOP-HSRL difference, measured as a percent of the mean HSRL AAC AOD of 0.047 (11%). The remaining source of error seems to be attributable to the spatial-temporal colocation of both instruments. While the CALIOP AAC AOD values show discrepancies with the coincident HSRL values, no particular bias is evident. This, unfortunately, prevents us from recommending any simple adjustment to obtain more accurate estimates of AAC AOD from the CALIOP data.

[49] Applying the depolarization ratio method to the coincident HSRL and CALIOP AAC data set leads to a very small number of cases ($N = 12$). Among those cases, only one data point is above the AOD daytime 99% confidence limit of 0.12 for the DR method. This is mainly due to (1) very few low opaque water clouds (needed to perform the DR retrieval) in our data set and (2) very few cases of CALIOP AAC detection above these clouds. We recall that flight dates and paths for HSRL underflights of CALIPSO were often chosen on the basis of optimizing boundary layer aerosol matchups and therefore biased to clear-sky conditions. The CALIOP DR AOD showed minimal discrepancies with either HSRL or CALIOP standard AOD values in the limited data set of our study. The very small number of suitable DR data points prevents us from recommending either the alternate DR or the standard CALIOP retrieval for a better detection of the AAC.

[50] We emphasize that our study is based on a limited number of coincident HSRL-CALIOP AAC cases, and the mean AAC AOD value of our data set can be lower by as much as half of the one over specific regions of high CALIOP AAC occurrence and intensity, such as offshore from the west coast of Africa in August–October 2007. We underline the need for additional suborbital field experiments in regions of high AAC occurrence (and intensity) to acquire knowledge on AAC

impacts such as process-level understanding of AAC aerosol-radiation interaction, cloud adjustments to the AAC aerosol-radiation interaction, or aerosol-cloud interaction. In addition, once the appropriate HSRL data sets become available, this will provide a higher number of coincident CALIOP-HSRL AAC cases with a wider AAC AOD range to further investigate the CALIOP standard and alternate detection and retrieval of AAC. Better identifying CALIOP's AAC observation capabilities over a wider range of aerosol conditions (i.e., different aerosol types and loadings) will contribute to a more accurate estimation of CALIOP-based global AAC radiative properties.

[51] **Acknowledgments.** This study was supported by CALIPSO ST funding under NASA grant NNX10AN60G. We would like to thank the CALIOP and HSRL teams for their efforts in providing and discussing these data sets.

References

Burton, S. P., R. A. Ferrare, C. A. Hostetler, J. W. Hair, R. R. Rogers, M. D. Obland, C. F. Butler, A. L. Cook, D. B. Harper, and K. D. Froyd (2012), Aerosol classification using airborne High Spectral Resolution Lidar measurements—Methodology and examples, *Atmos. Meas. Tech.*, *5*, 73–98, www.atmos-meas-tech.net/5/73/2012/, doi:10.5194/amt-5-73-2012.

Burton, S. P., R. A. Ferrare, M. A. Vaughan, A. H. Omar, R. R. Rogers, C. A. Hostetler, and J. W. Hair (2013), Aerosol classification from airborne HSRL and comparisons with the 1 CALIPSO vertical feature mask, *Atmos. Meas. Tech. Discuss.*, *6*, 1815–1858, doi:10.5194/amtd-6-1815-2013.

Cattrall, C., J. Reagan, K. Thome, and O. Dubovik (2005), Variability of aerosol and spectral lidar and backscatter and extinction ratios of key aerosol types derived from selected Aerosol Robotic Network locations, *J. Geophys. Res.*, *110*, D10S11, doi:10.1029/2004JD005124.

Chand, D., T. L. Anderson, R. Wood, R. J. Charlson, Y. Hu, Z. Liu, and M. Vaughan (2008), Quantifying above-cloud aerosol using spaceborne lidar for improved understanding of cloudy-sky direct climate forcing, *J. Geophys. Res.*, *113*, D13206, doi:10.1029/007JD009433.

Chand, D., R. Wood, T. L. Anderson, S. K. Satheesh, and R. J. Charlson (2009), Satellite-derived direct radiative effect of aerosols dependent on cloud cover, *Nat. Geosci.*, *2*, 181–184, doi:10.1038/ngeo437.

Chylek, P., and J. Wong (1995), Effect of absorbing aerosols on global radiation budget, *Geophys. Res. Lett.*, *22*, 929–931.

Coddington, O., P. Pilewskie, J. Redemann, S. Platnick, P. Russell, K. Schmidt, W. Gore, J. Livingston, G. Wind, and T. Vukicevic (2010), Examining the impact of overlying aerosols on the retrieval of cloud optical properties from passive remote sensing, *J. Geophys. Res.*, *115*, D10211, doi:10.1029/2009JD012829.

Davis, K. J., N. Gamage, C. R. Hagelberg, C. Kiemle, D. H. Lenschow, and P. P. Sullivan (2000), An objective method for deriving atmospheric structure from airborne lidar observations, *J. Atmos. Oceanic Technol.*, *17*, 1455–1468.

De Graff, M., L. G. Tilstra, P. Wang, and P. Stammes (2012), Retrieval of the aerosol direct radiative effect over clouds from spaceborne spectrometry, *J. Geophys. Res.*, *117*, D07207, doi:10.1029/2011JD017160.

Devasthale, A., and M. A. Thomas (2011), A global survey of aerosol-liquid water cloud overlap based on four years of CALIPSO–CALIOP data, *Atmos. Chem. Phys.*, *11*, 1143–1154.

Hair, J. W., L. M. Caldwell, D. A. Krueger, and C. Y. She (2001), High-spectral-resolution lidar with iodine-vapor filters: Measurement of atmospheric-state and aerosol profiles, *Appl. Optics*, *40*, 5280–5294.

Hair, J. W., C. A. Hostetler, A. L. Cook, D. B. Harper, R. A. Ferrare, T. L. Mack, W. Welch, L. R. Isquierdo, and F. E. Hovis (2008), Airborne high spectral resolution lidar for profiling aerosol optical properties, *Appl. Optics*, *47*, 6734–6752, doi:10.1364/AO.47.006734.

Haywood, J. M., and K. P. Shine (1995), The effect of anthropogenic sulfate and soot aerosol on the clear sky planetary radiation budget, *Geophys. Res. Lett.*, *22*, 603–606.

Haywood, J. M., S. R. Osborne, and S. J. Abel (2004), The effect of overlying absorbing aerosol layers on remote sensing retrievals of cloud effective radius and cloud optical depth, *Q. J. R. Meteorol. Soc.*, *130*, 779–800.

Hu, Y., Z. Liu, D. Winker, M. Vaughan, V. Noel, L. Bissonnette, G. Roy, and M. McGill (2006), A simple relation between lidar multiple scattering and depolarization for water clouds, *Opt. Lett.*, *31*(12), 1809–1811.

Hu, Y., M. Vaughan, Z. Liu, K. Powell, and S. Rodier (2007a), Retrieving optical depths and lidar ratios for transparent layers above opaque water clouds from CALIPSO lidar measurements, *IEEE Geosci. Remote Sens. Lett.*, *4*, 523–526, doi:10.1109/LGRS.2007.901085.

Hu, Y. M. V., et al. (2007b), The depolarization-attenuated backscatter relation: CALIPSO lidar measurements vs. theory, *Opt. Express*, *15*, 5327–5332, doi:10.1364/OE.15.005327.

Hunt, W. H., D. M. Winker, M. A. Vaughan, K. A. Powell, P. L. Lucker, and C. Weimer (2009), CALIPSO lidar description and performance assessment, *J. Atmos. Oceanic Technol.*, *26*, 1214–1228, doi:10.1175/2009JTECHA1223.1.

Jethva, H., O. Torres, L. A. Remer, and P. K. Bhartia (2013), A color ratio method for simultaneous retrieval of aerosol and cloud optical thickness of above-cloud absorbing aerosols from passive sensors: Application to MODIS measurements, *IEEE Trans. Geosci. Remote Sens.*, *99*, 1–9.

Justice, C. O., L. Giglio, S. Korontzi, J. Owens, J. T. Morisette, D. Roy, J. Descloitres, S. Alleaume, F. Petitcolin, and Y. Kaufman (2002), The MODIS fire products, *Remote Sens. Environ.*, *83*, 244–262.

Kacenelenbogen, M., M. A. Vaughan, J. Redemann, R. M. Hoff, R. R. Rogers, R. A. Ferrare, P. B. Russell, C. A. Hostetler, J. W. Hair, and B. N. Holben (2011), An accuracy assessment of the CALIOP/CALIPSO version 2/version 3 daytime aerosol extinction product based on a detailed multi-sensor, multi-platform case study, *Atmos. Chem. Phys.*, *11*, 3981–4000, doi:10.5194/acp-11-3981-2011.

Kim, S.-W., S. Berthier, J.–C. Raut, P. Chazette, F. Dulac, and S.– C. Yoon (2008), Validation of aerosol and cloud layer structures from the space-borne lidar CALIOP using a ground-based lidar in Seoul, Korea, *Atmos. Chem. Phys.*, *8*, 3705–3720.

Kinne, S. (2009), Remote sensing data combinations-superior global maps for aerosol optical depth, in *Satellite Aerosol Remote Sensing Over Land*, edited by A. Kokhanovsky and G. de Leeuw, pp. 361–381, Springer, Berlin Heidelberg.

Klein, S. A., and D. L. Hartmann (1993), The seasonal cycle of low stratiform clouds, *J. Clim.*, *6*, 1587–1606, doi:10.1175/1520-0442(1993)006<1587:TSCOLS>2.0.CO;2.

Knobelspiesse, K., B. Cairns, J. Redemann, R. W. Bergstrom, and A. Stohl (2011), Simultaneous retrieval of aerosol and cloud properties during the MILAGRO field campaign, *Atmos. Chem. Phys.*, *11*, 6245–6263.

Koch, D., and A. D. Del Genio (2010), Black carbon semi-direct effects on cloud cover: Review and synthesis, *Atmos. Chem. Phys.*, *10*, 7685–7696.

Liu, Z., R. Kuehn, M. Vaughan, D. Winker, A. Omar, K. Powell, C. Trepte, Y. Hu, and C. Hostetler (2010), The CALIPSO cloud and aerosol discrimination: Version 3, Algorithm and test results, 25th International Laser and radar conference.

Mielonen, T., A. Arola, M. Komppula, J. Kukkonen, J. Koskinen, G. de Leeuw, and K. E. J. Lehtinen (2009), Comparison of CALIOP level 2 aerosol subtypes to aerosol types derived from AERONET inversion data, *Geophys. Res. Lett.*, *36*, L18804, doi:10.1029/2009GL039609.

O'Connor, E. J., A. J. Illingworth, and R. J. Hogan (2004), A technique for autocalibration of cloud lidar, *J. Atmos. Oceanic Technol.*, *21*, 777–786, doi:10.1175/1520-0426(2004)021<0777:ATFAOC>2.0.CO;2.

Omar, A. H., J.-G. Won, D. M. Winker, S.–C. Yoon, O. Dubovik, and M. P. McCormick (2005), Development of global aerosol models using cluster analysis of Aerosol Robotic Network (AERONET) measurements, *J. Geophys. Res.*, *110*, D10S14, doi:10.1029/2004JD004874.

Omar, A., et al. (2009), The CALIPSO automated aerosol classification and lidar ratio selection algorithm, *J. Atmos. Oceanic Technol.*, *26*, 1994–2014, doi:10.1175/2009JTECHA1231.1.

Pappalardo, G., et al. (2010), EARLINET correlative measurements for CALIPSO: First intercomparison results, *J. Geophys. Res.*, *115*, D00H19, doi:10.1029/2009JD012147.

Piironen, P., and E. W. Eloranta (1994), Demonstration of a high-spectral-resolution lidar based on an iodine absorption filter, *Opt. Lett.*, *19*, 234–236.

Pinnick, R. G., S. G. Jennings, P. Chylek, C. Ham, and W. T. Grandy Jr. (1983), Backscatter and extinction in water clouds, *J. Geophys. Res.*, *88*, 6787–6796, doi:10.1029/JC088iC11p06787.

Platt, C. M. (1973), Lidar and radioinetric observations of cirrus clouds, *J. Atmos. Sci.*, *30*, 1191–1204.

Platt, C. M. R., D. M. Winker, M. A. Vaughan, and S. D. Miller (1999), Backscatter to extinction ratios in the top layers of tropical mesoscale convective systems and in isolated cirrus from LITE observations, *J. Appl. Meteorol.*, *38*, 1330–1345, doi:10.1175/1520-0450(1999)038<1330:BTERIT>2.0.CO;2.

Redemann, J., P. Pilewskie, P. B. Russell, J. M. Livingston, S. Howard, B. Schmid, J. Pommier, W. Gore, J. Eilers, and M. Wendisch (2006), Airborne measurements of spectral direct aerosol radiative forcing in the intercontinental chemical transport experiment/intercontinental transport and chemical transformation of anthropogenic pollution, 2004, *J. Geophys. Res.*, *111*, D14210, doi:10.1029/2005JD006812.

Remer, L. A. (2009), Atmospheric science: Smoke above clouds, *Nat. Geosci.*, *2*, 167–168, doi:10.1038/ngeo456.

Remer, L. A., et al. (2008), Global aerosol climatology from the MODIS satellite sensors, *J. Geophys. Res.*, *113*, D14S07, doi:10.1029/2007JD009661.

Rogers, R. R., et al. (2011), Assessment of the CALIPSO Lidar 532 nm attenuated backscatter calibration using the NASA LaRC airborne High Spectral Resolution Lidar, *Atmos. Chem. Phys.*, *11*, 1295–1311, doi:10.5194/acp-11-1295-2011.

Russell, P. B., S. Kinne, and R. Bergstrom (1997), Aerosol climate effects: Local radiative forcing and column closure experiments, *J. Geophys. Res.*, *102*, 9397–9407.

Russell, P. B., et al. (2002), Comparison of aerosol single scattering albedos derived by diverse techniques in two North Atlantic experiments, *J. Atmos. Sci.*, *59*, 609–619.

Sakaeda, N., R. Wood, and P. J. Rasch (2011), Direct and semidirect aerosol effects of southern African biomass burning aerosol, *J. Geophys. Res.*, *116*, D12205, doi:10.1029/2010JD015540.

Schuster, G. L., M. Vaughan, D. MacDonnell, W. Su, D. Winker, O. Dubovik, T. Lapyonok, and C. Trepte (2012), Comparison of CALIPSO aerosol optical depth retrievals to AERONET measurements, and a climatology for the lidar ratio of dust, *Atmos. Chem. Phys.*, *12*, 7431–7452, doi:10.5194/acp-12-7431-2012.

Shinozuka, Y., and J. Redemann (2011), Horizontal variability of aerosol optical depth observed during the ARCTAS airborne experiment, *Atmos. Chem. Phys.*, *11*, 8489–8495, doi:10.5194/acp-11-8489-2011.

Torres, O., J. Hiren, and P. K. Bhartia (2012), Retrieval of aerosol optical depth above clouds from OMI observations: Sensitivity analysis and case studies. *J. Atmos. Sci.*, *69*, 1037–1053.

Várnai, T. and A. Marshak (2009), MODIS observations of enhanced clear sky reflectance near clouds, *Geophys. Res. Lett.*, *36*, L06807, doi:10.1029/2008GL037089.

Vaughan, M. A., D. M. Winker, and K. A. Powell (2005), CALIOP algorithm theoretical basis document, Part 2: Feature detection and layer properties algorithms, PC-SCI-202.01, NASA Langley Research Center, Hampton, VA 23681, 87 pp. [Available online at http://www-calipso.larc.nasa.gov/resources/project_documentation.php].

Vaughan, M., K. Powell, R. Kuehn, S. Young, D. Winker, C. Hostetler, W. Hunt, Z. Liu, M. McGill, and B. Getzewich (2009), Fully automated detection of cloud and aerosol layers in the CALIPSO lidar measurements, *J. Atmos. Oceanic Technol.*, *26*, 2034–2050, doi:10.1175/2009JTECHA1228.1.

Waquet, F., J. Riedi, L. C. Labonnote, P. Goloub, B. Cairns, J.-L. Deuzé, and D. Tanré (2009), Aerosol remote sensing over clouds using A-train observations, *J. Atmos. Sci.*, doi:10.1175/2009JAS3026.1.

Waquet, F., et al. (2012), Retrieval of aerosol microphysical and optical properties above liquid clouds from POLDER/PARASOL polarization measurements, *Atmos. Meas. Tech. Discuss.*, *5*, 6083–6145, doi:10.5194/amtd-5-6083-2012.

Wen, G., A. Marshak, R. F. Cahalan, L. A. Remer, and R. G. Kleidman (2007), 3-D aerosol–cloud radiative interaction observed in collocated MODIS and ASTER images of cumulus cloud fields, *J. Geophys. Res.*, *112*, D13204, doi:10.1029/2006JD008267.

Wilcox, E. M. (2010), Stratocumulus cloud thickening beneath layers of absorbing smoke aerosol, *Atmos. Chem. Phys.*, *10*, 11,769–11,777.

Wilcox, E. M., H. Vardhan, and S. Platnick (2009), Estimate of the impact of absorbing aerosol over cloud on the MODIS retrievals of cloud optical thickness and effective radius using two independent retrievals of liquid water path, *J. Geophys. Res.*, *114*, D05210, doi:10.1029/2008JD010589.

Winker, D. M., M. A. Vaughan, A. Omar, Y. Hu, K. A. Powell, Z. Liu, W. H. Hunt, and S. A. Young (2009), Overview of the CALIPSO mission and CALIOP data processing algorithms, *J. Atmos. Oceanic Technol.*, *26*, 2310–2323, doi:10.1175/2009JTECHA1281.1.

Winker, D. M., J. L. Tackett, B. J. Getzewich, Z. Liu, M. A. Vaughan, and R. R. Rogers (2013), The global 3-D distribution of tropospheric aerosols as characterized by CALIOP, *Atmos. Chem. Phys.*, *13*, 3345–3361, doi:10.5194/acp-13-3345-2013.

Wood, R. (2012), Stratocumulus clouds, *Mon. Weather Rev.*, *140*, 2373–2423, doi:10.1175/MWR-D-11-00121.1.

Young, S. A., and M. A. Vaughan (2009), The retrieval of profiles of particulate extinction from Cloud Aerosol Lidar Infrared Pathfinder Satellite Observations (CALIPSO) data: Algorithm description, *J. Atmos. Oceanic Technol.*, *26*, 1105–1119, doi:10.1175/2008JTECHA1221.1.

Yu, H., and Z. Zhang (2013), New directions: Emerging satellite observations of above-cloud aerosols and direct radiative forcing, *Atmos. Environ.*, *72*, 36–40, doi:10.1016/j.atmosenv.2013.02.017.

Yu, H., Y. Zhang, M. Chin, Z. Liu, A. Omar, L. A. Remer, Y. Yang, T. Yuan, and J. Zhang (2012), An integrated analysis of aerosol above clouds from A-Train multi-sensor measurements, *Remote Sens. Environ.*, *121*: 125–131.

Zhang, J., J. S. Reid, and B. N. Holben (2005), An analysis of potential cloud artifacts in MODIS over ocean aerosol optical thickness products, *Geophys. Res. Lett.*, *32*, L15803, doi: 10.1029/2005GL023254.